Inorganic Chemistry

Article

pubs.acs.org/IC

Solid-State NMR and Raman Spectroscopy To Address the Local Structure of Defects and the Tricky Issue of the Cu/Zn Disorder in Cu-Poor, Zn-Rich CZTS Materials

Michaël Paris,* Léo Choubrac, Alain Lafond, Catherine Guillot-Deudon, and Stéphane Jobic

Institut des Matériaux Jean Rouxel (IMN), Université de Nantes, CNRS, 2, rue de la Houssinière, BP 32229, 44322 Nantes Cedex 03, France

Supporting Information

ABSTRACT: The material $Cu_2ZnSn(S,Se)_4$ (CZTS) offers a promising indium-free alternative to $Cu(In,Ga)Se_2$ for the absorber layer in thin-film solar cells. It is known that the highest solar energy conversion efficiencies are reached for Cu-poor, Zn-rich CZTS compositions and that too much disorder at the Cu and Zn sites can have a negative impact on the device performance. In this article, we investigate the structures of $[V_{Cu} + Zn_{Cu}]$ A-type and $[2Zn_{Cu} + Zn_{Sn}]$ B-type defect complexes and their impact on the long-range Cu/Zn disorder. To that end, we use ^{119}Sn, ^{65}Cu, and ^{67}Zn solid-state NMR and Raman spectroscopy to characterize powdered CZTS samples. For both A- and B-type substitutions, our NMR investigations demonstrate the clustering of the complexes. Moreover, we show that (A+B)-type compounds should be considered as A-type and B-type compounds, since no interaction seems to exist between $[V_{Cu} + Zn_{Cu}]$ and $[2Zn_{Cu} + Zn_{Sn}]$ defect complexes. In addition, it is worth noting that $[2Zn_{Cu} + Zn_{Sn}]$ complexes have only a minor impact on the level of disorder at the Cu and Zn sites. In contrast, $[V_{Cu} + Zn_{Cu}]$ complexes seem to restrain the random distribution of Cu at the Zn site and of Zn at the Cu site; i.e., the long-range Cu/Zn disorder. Raman characterization of the CZTS samples was also conducted. The $Q = I_{287}/I_{303}$ and the newly introduced $Q' = I_{338}/(I_{366} + I_{374})$ ratios determined from Raman spectra collected at 785 nm turn out to be very sensitive to the level of Cu/Zn disorder. Moreover, they can be used to differentiate the nature of the substitution in slow-cooled materials.

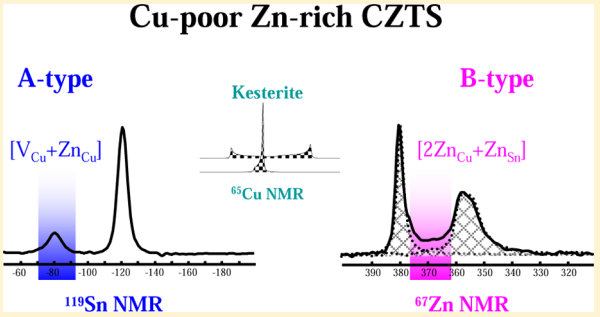

INTRODUCTION

The material $Cu_2ZnSn(S,Se)_4$ (CZTS) offers a promising indium-free alternative to $Cu(In,Ga)Se_2$ (CIGS) for the absorber layer in thin-film solar cells. Although solar energy conversion up to 12.6% has been recently achieved with a mixed sulfo-selenide CZTS absorber,[1] huge improvements are still needed to reach the 20% efficiencies of CIGS-based solar cells.[2] Currently, theoretical and experimental investigations have highlighted the possible negative effects of Cu/Zn disorder, i.e. the overall random distribution of Cu and Zn at both Cu and Zn sites, on the CZTS-based solar cell performances.[3,4] Furthermore, it was experimentally demonstrated that Cu-poor, Zn-rich compositions offer better photovoltaic performances. A detailed understanding of such behavior is still lacking, even though Chen et al.[5] suggested, from theoretical calculations, that Cu-poor, Zn-rich compositions are beneficial because they make V_{Cu} and Zn_{Cu} the dominant defects. These observations are indicative of the absolute need to find out clear relationships between the structure and photoelectronic properties of CZTS materials to improve the performance of CZTS-based solar cells in the foreseeable future. In that framework, we have embarked on the characterization of defect complexes and the elucidation of their influence on the long-range Cu/Zn random distribution.

It is now well established that stoichiometric CZTS compounds adopt either an ordered or a disordered kesterite structure type, depending on the synthesis conditions. Both structure types can be regarded as derivatives of the cubic sphalerite ZnS structure (doubling of one parameter of the subcell with all cations in tetrahedral sites) with a long-range stacking of [Cu,Sn] and [Cu,Zn] layers along the *c* axis of the tetragonal cell. In the ordered variant, all cationic species occupied specific Wyckoff positions of the $I\bar{4}$ space group (SG), i.e. Cu at 2a and 2c sites, and Sn and Zn at 2b and 2d sites, respectively (Figure 1).[6,7] In the disordered variant, both Cu and Zn can be distributed over the 2c and 2d sites, leading to a change in the SG from $I\bar{4}$ to $I\bar{4}2m$ if the distribution is fully random (Figure 1). Discrimination between the ordered and disordered kesterite structures is not feasible by conventional X-ray diffraction experiments (XRD) because Cu and Zn have nearly identical X-ray scattering factors. Fortunately, we have shown recently that a local probe technique such as solid-state

Received: May 29, 2014
Published: July 29, 2014

   dx.doi.org/10.1021/ic5012346 | Inorg. Chem. 2014, 53, 8646−8653

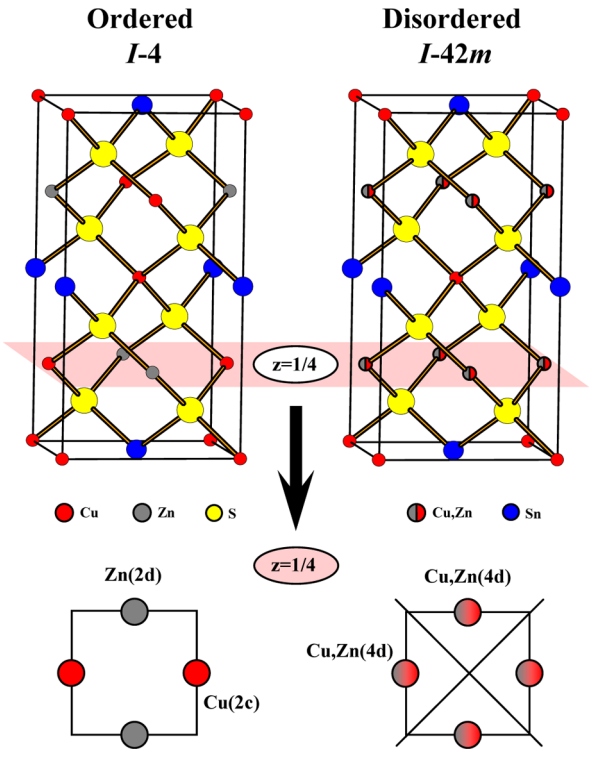

Figure 1. Representations of the ordered ($I\bar{4}$) and disordered ($I\bar{4}2m$) CZTS kesterite structures. In contrast with the stannite structure, the 2a site is only occupied by Cu atoms for the two kesterite structures. An enlarged and detailed figure is available in the Supporting Information with a list of the first cationic neighbors for the ordered structure.

nuclear magnetic resonance (NMR) (with ^{65}Cu, ^{67}Zn, and ^{119}Sn as probes) is a very efficient tool to tackle such a Cu/Zn disorder in stoichiometric CZTS samples.[8] For convenience, the $I\bar{4}$ SG will be used hereafter for discussions of the results.

Most of the realistic substitutions in off-stoichiometric CZTS have already been discussed.[9,10] So far, two main substitutions have been considered in Cu-poor CZTS materials: namely, the A-type substitution $2Cu \rightarrow V_{Cu} + Zn_{Cu}$ ($[V_{Cu} + Zn_{Cu}]$ complex) and the B-type substitution $2Cu + Sn \rightarrow 2Zn_{Cu} + Zn_{Sn}$ ($[2Zn_{Cu} + Zn_{Sn}]$ complex), with their (A+B) combinations. The characterization of these defect complexes through a global and long-range technique is still challenging.

Consequently, the goal of this work is to give a deeper understanding of the local structure associated with the A-type, B-type, and the (A+B)-type substitutions. Samples with a given stoichiometry were prepared with a control of the Cu/Zn disorder via the choice of the appropriate thermal treatment and were analyzed by ^{67}Zn, ^{119}Sn, and ^{65}Cu NMR spectroscopy and Raman spectroscopy. In the Results and Discussion, we establish first a relationship among the characteristics of the NMR signals, the nature of the defect complexes, and the Cu/Zn disorder. On the basis of these results, we extend our investigations to Raman spectroscopy, a technique more convenient than NMR for characterization of thin films. At this stage, we can anticipate that these investigations carried out on bulk materials will be used as reference for future actions on thin-film layers.

EXPERIMENTAL SECTION

Synthesis. Stoichiometric CZTS (Cu_2ZnSnS_4, S sample), A-type ($Cu_{2-2x}Zn_{1+x}SnS_4$, A sample), B-type ($Cu_{2-2y}Zn_{1+3y}Sn_{1-y}S_4$, B sample), and (A+B)-type ($Cu_{2-2x-2y}Zn_{1+x+3y}Sn_{1-y}S_4$, (A+B) sample) materials were prepared via a ceramic route at 750 °C according to Bernardini et al.[11] (details are given in the Supporting Information). To shed light on the relationship between chemical composition and Cu/Zn disorder, the strategy used previously with success for probing disorder in stoichiometric CZTS compounds[8] was applied. Practically, each sample was divided into two batches. Both were annealed at 750 °C in quartz ampules under vacuum, and one was ice-quenched (Q) while the second was cooled to 10 °C/h (S). The so-obtained samples are hereafter labeled X_Q and X_S, where X stands for the composition type (X = S, A, B or A+B). For example, S_S refers to the slow-cooled stoichiometrically prepared sample. X_Q compounds are expected to be much more disordered (Cu/Zn disorder) than X_S compounds for thermodynamic reasons.

Chemical Composition of Prepared Materials. Accurate chemical compositions of the studied materials were determined by energy-dispersive X-ray spectroscopy carried out on polished sections using a set of CZTS samples as internal standards (details are given in the Supporting Information). These standards were previously calibrated accurately from electron probe microanalyses.[12] At least 10 spot analyses (10^6 counts/spectrum) on different areas of the probed pellets (beam diameter ~2 μm) were collected for each batch. Average values for the chemical composition of the CZTS phase are reported in Table 1 and assigned to S, A, B, and A+B type versus the experimental composition.

Table 1. Experimental Compositions of Prepared Samples and Numbers of Sn Atoms Affected per Cu Vacancy for A-Type Defect Complexes Issued from the Examination of ^{119}Sn NMR Spectra

	composition $Cu_XZn_YSn_ZS_4$[a]			A-type Cu vacancy[b]		
sample	X	Y	Z	V (%)	I (%)	$N = I/V$
S_S	1.97	1.01	1.01			
A_S	1.84	1.08	1.01	7	11	1.6
$(A+B)_S$	1.75	1.15	0.99	11	25	2.3
B_S	1.95	1.06	0.99			
S_Q	1.98	1.01	1.01			
A_Q	1.82	1.08	1.00	10	16	1.6
$(A+B)_Q$	1.79	1.14	0.99	8	15	1.9
B_Q	1.96	1.06	0.99			

[a]The estimated deviation of the X, Y, and Z values is 0.01. [b]V is the fraction of V_{Cu} at the 2a site calculated as $4 - X - Y - Z$. I is the intensity of the ^{119}Sn NMR line at −81 ppm relative to the whole spectrum. $N = I/V$ is the actual number of Sn atoms affected per Cu vacancy.

Solid-State Nuclear Magnetic Resonance. The ^{119}Sn ($I = {}^1/_2$), ^{65}Cu ($I = {}^3/_2$), and ^{67}Zn ($I = {}^5/_2$) NMR spectra were acquired on two Bruker Avance III 300 and 500 MHz spectrometers with 4 mm CP-MAS probes. Rotors were spun at 14 kHz and 10 kHz for ^{119}Sn and ^{67}Zn spectra, respectively. ^{65}Cu spectra were acquired under static conditions, giving more reliable (NMR parameter derivations) and more easily comprehensible spectra.[8] To obtain an absorption mode only line shape, both ^{119}Sn and ^{65}Cu spectra were carried out using a full shifted echo acquisition ($\theta - \tau - 2\theta -$ acq). For ^{119}Sn, τ was set to 1.9 ms and θ to $\pi/2$ for an radio frequency (RF) field of 80 kHz. We ensured the quantitative feature of these ^{119}Sn echo spectra by comparison with direct excitation spectra. For ^{65}Cu, we used $\theta = \pi/10$ for a RF field of 35 kHz and τ =1.2 ms, except for the S_Q sample, for which τ =1.0 ms. ^{67}Zn magic angle spinning (MAS) spectra were acquired with a rotor synchronized Hahn echo sequence ($\pi/6 - \tau - \pi/3 - \tau -$ acq) with τ equal to one rotor period and a RF field of 23 kHz. To improve the signal-to-noise ratio of the ^{67}Zn spectrum of A_Q,

dx.doi.org/10.1021/ic5012346 | Inorg. Chem. 2014, 53, 8646−8653

we used a convergent double-frequency sweep[13] prior to the Hahn echo sequence. The sweep duration was 4 ms for a RF field of 23 kHz and ran from 700 to 10 kHz. Recycle times were 120, 1, and 2 s for ^{119}Sn, ^{65}Cu, and ^{67}Zn, respectively. Spectra were referenced at 0 ppm against solid-state CuCl for ^{65}Cu and a $Zn(NO_3)_2$(aq) solution for ^{67}Zn. Finally, ^{119}Sn spectra were referenced to Me_4Sn using Ph_4Sn as a secondary reference (−121.15 ppm). All spectral decompositions were done using the "dmfit" freeware.[14]

Raman Spectroscopy. Raman spectra recorded at 514.5 nm excitation wavelength were acquired in backscattering configuration on a Jobin-Yvon T64000 spectrometer coupled to a microscope (spot surface ∼5 μm^2). A Renishaw InVia Reflex spectrometer was used for measurements at 785 nm excitation wavelength (spot surface ∼1 μm^2). Frequencies were calibrated using the Si band at 520.5 cm^{-1}. As the laser excitation could induce modifications of the spectra (thermal effects and/or ordered to disordered phase transition within the kesterite structure) as reported by Valakh et al.,[15] all measurements were performed with low power density of the incident laser, 0.02 and 0.5 mW/μm^2, for the 514 and 785 nm excitation wavelengths, respectively.

RESULTS AND DISCUSSION

This section is organized as follows. The ^{119}Sn, ^{67}Zn, and ^{65}Cu NMR characterizations of the low-disordered samples (i.e., slow-cooled CZTS samples) with clear spectral signatures of $[V_{Cu} + Zn_{Cu}]$ and $[2Zn_{Cu} + Zn_{Sn}]$ defect complexes are discussed in the first part. Thereafter, the A, B, and (A+B) substitution types are addressed first separately through the examination of their ^{67}Zn and ^{119}Sn NMR spectra (Figures 2 and 3, respectively). Then, ^{65}Cu NMR spectra are interpreted for all of the samples (Figure 4). The second part is devoted to strongly disordered materials (i.e., fast-cooled CZTS samples). Both parts deal with the relation between the long-range Cu/Zn disorder and the A and B substitution types. In a third part, the use of Raman spectroscopy to probe both the cationic ordering in CZTS and the nature of the substitution is emphasized.

Characterization of the Substitutions in Low-Disordered Samples by NMR. *A-Type Substitution in $Cu_{1.84(1)}Zn_{1.08(1)}Sn_{1.01(1)}S_4$ (Sample A_S).* On the basis of an examination of Figure 2, it appears that the ^{67}Zn MAS spectra of the S_S (used as reference) and A_S samples are very similar. Both exhibit a single line at 355 ppm characteristic of Zn atoms experiencing a small electric field gradient (EFG): i.e., a quadrupolar coupling constant of about 1 MHz. This line was previously assigned to Zn atoms exclusively localized on the [Cu,Zn] layers of the kesterite structure of CZTS.[8] No Zn atom located at the 2a site is detected. This conclusion fully agrees with anomalous powder XRD carried out on copper-poor, zinc-rich CZTS powder that concluded in the preferential positioning of copper vacancies and extra Zn atoms at the 2a and 2c sites, respectively ($Cu(2a) + Cu(2c) \rightarrow V_{Cu}(2a) + Zn_{Cu}(2c)$).[9]

Because tin is a heavy atom, the chemical shift of the ^{119}Sn NMR line is expected to be much more sensitive to changes in the chemical surroundings in the second coordination shell than the ^{67}Zn chemical shift is. An examination of Figure 3 shows that the main ^{119}Sn NMR line peaking at −121 ppm for A_S is narrower than the line peaking at −122 ppm for S_S. On the basis of our previous interpretation of the ^{119}Sn signal modifications with Cu/Zn disorder in stoichiometric CZTS samples,[8] this shows that the A_S compound contains fewer $[Cu_{Zn} + Zn_{Cu}]$ defect complexes than the S_S compound, this latter never being totally free of such complexes (even for samples cooled very slowly), as already pointed out by neutron investigation[7] and solid-state NMR.[8] However, the most striking difference between the ^{119}Sn NMR spectra of A_S and S_S lies in the appearance of an additional line at −81 ppm for the Cu-poor sample. Considering that A_S is less disordered than S_S and that no additional ^{119}Sn line was previously observed in highly disordered stoichiometric samples,[8] we conclude that the $[Cu_{Zn} + Zn_{Cu}]$ defect complexes cannot be responsible for the −81 ppm resonance. Thus, we propose to assign this specific line to ^{119}Sn nuclei (at the 2b site) experiencing the presence of Cu vacancies ($V_{Cu}(2a)$, as suggested by Lafond et al.[9]) in its second coordination shell. This attribution is further supported by the rise in line intensity with the amount of Cu vacancies (0, 5, 7, and 11%) in a series of four samples cooled under the same conditions (Supporting Information, Figure S2).

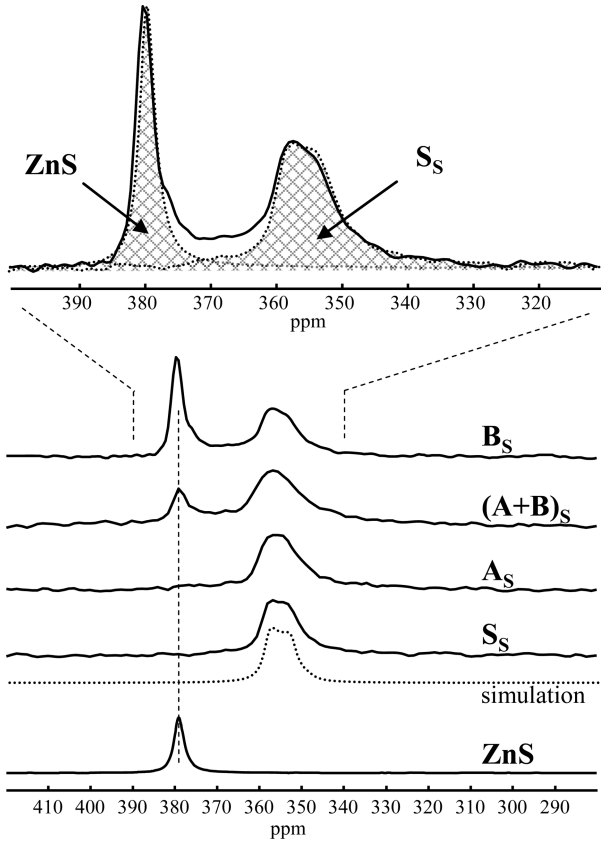

Figure 2. ^{67}Zn central transition (Hahn echo acquisition) MAS (10 kHz) NMR spectra acquired at 31.3 MHz (11.75 T) of the S_S, A_S, $(A+B)_S$, B_S, and cubic ZnS samples. The simulation of the S_S spectrum by a single line, whose line shape results from the second-order contribution of a weak quadrupolar interaction (quadrupolar coupling constant of 1 MHz), is given by the dotted line. The upper part of the figure corresponds to an enlargement of the spectrum of B_S, along with shaded areas corresponding to the spectra of ZnS and S_S. The difference highlights the specific signature of B-type complexes.

Formally, with regard to the kesterite structure, each copper vacancy at a 2a site (i.e., within the [Cu,Sn] layer) should directly affect up to four surrounding tin atoms (Supporting Information, Figure S3). Consequently, according to the composition of the A_s sample (Table 1) for which the percentage of copper vacancies (V) equals 7%, a model involving only isolated $[V_{Cu}(2a) + Zn_{Cu}(2c)]$ defect complexes should perturb 28% of the Sn atoms (i.e., V multiplied by 4). As the relative intensity of the NMR signal at −81 ppm represents

dx.doi.org/10.1021/ic5012346 | Inorg. Chem. 2014, 53, 8646−8653

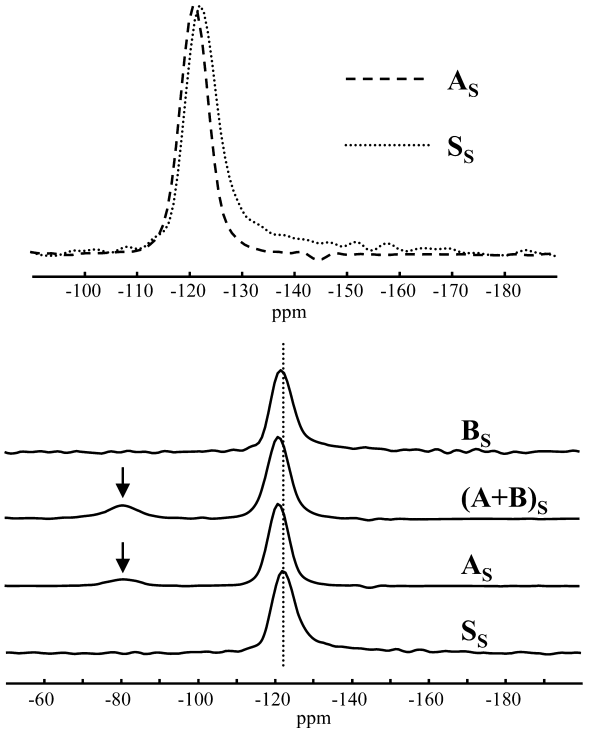

Figure 3. ^{119}Sn (full shifted echo acquisition) MAS (14 kHz) NMR spectra acquired at 111.9 MHz (7.05 T) of the S_S, A_S, $(A+B)_S$, and B_S samples. Arrows indicate the additional signal assigned to ^{119}Sn nuclei experiencing the presence of Cu vacancies in the [Cu,Sn] layers of the CZTS structure. The upper part of the figure points out the difference in line widths for the −121 ppm resonance of the A_S and S_S samples.

only 11% of the whole ^{119}Sn spectrum, it can be concluded that copper vacancies in A_S affect much fewer Sn atoms than expected (1.6 Sn/V_{Cu} vs 4.0 Sn/V_{Cu}). This clearly indicates that the A-type complexes have the strong propensity to segregate. This is in full agreement with theoretical investigations that anticipated the clustering of A-type defect complexes, the formation energy of such conglomerates being lower than that of multiple isolated defect complexes.[16] This observation can be extended to all materials with A-type defect complexes (see *N* values in Table 1). Moreover, the width of the line at −81 ppm is similar to the width of the main signal at −121 ppm. This strongly suggests that the aggregation of [V_{Cu} + Zn_{Cu}] complexes results at the end in a reproducible and structurally well-defined arrangement.

B-Type Substitution in $Cu_{1.95(1)}Zn_{1.06(1)}Sn_{0.99(1)}S_4$ (Sample B_S). The B-type substitution with [$2Zn_{Cu}$ + Zn_{Sn}] defect complexes leads locally to Sn-poor, Zn-rich zones. There, tin atoms turn out to be too far away from Zn_{Sn} defects to induce modifications in the ^{119}Sn NMR spectrum of B_S in comparison to that of S_S (Figure 1). This assertion is confirmed by an examination of Figure 3. Moreover, on the basis of ^{119}Sn line width, B_S presents a degree of disorder in the [Cu,Zn] layer similar to that of S_S. This is in contrast with A_S, which was shown to be the most ordered.

Moreover, the ^{67}Zn spectrum of the B_S sample in Figure 2 reveals a very new, broad, and diffuse signal surrounded by the contributions of CZTS at 355 ppm[8] and ZnS impurities at 379 ppm.[17,18] The signal between these two aforementioned borders can be considered the signature of the B-type substitution. It does not exhibit a line shape characteristic of the second-order quadrupolar interaction under MAS conditions and, consequently, has to be ascribed to Zn atoms experiencing different chemical surroundings. Namely, each [ZnS_4] tetrahedron is surrounded by 12 identical tetrahedra in cubic ZnS, which give rise to an intense and sharp NMR peak at 379 ppm. In the ordered kesterite structure, a zinc atom (at the 2d site) has eight copper and four tin atoms as second neighbors, leading to a wider NMR peak at 355 ppm (Supporting Information, Figure S4). Let us first deal with a single B-type complex. When the B-type substitution occurs, two copper atoms and one tin atom are replaced by three zinc atoms ($2Cu + Sn \rightarrow 2Zn_{Cu} + Zn_{Sn}$). To respect the charge balance at the local scale, Zn at Cu sites and Zn at Sn sites will attract each other. Consequently, the major part of [ZnS_4] tetrahedra is linked to [CuS_4] and [SnS_4] tetrahedra, but the secondary coordination shell of some of them is singularly Zn enriched, up to six Zn atoms (Supporting Information, Figure S4). When several B-type complexes are combined, the coordination shell of some cations may contain more than six Zn atoms. Thus, we suggest that the specific B-type signal originates from a distribution of isotropic chemical shifts reflecting variations in the chemical surroundings of Zn nuclei. This speculation goes along with the likely conglomeration of defect complexes, since Zn chemical environments almost similar to those in ZnS are detectable: i.e., nearly 12 Zn atoms as second neighbors.

(A+B)-Type Substitution in $Cu_{1.75(1)}Zn_{1.15(1)}Sn_{0.99(1)}S_4$ (Sample $(A+B)_S$). The $(A+B)_S$ compound presents the same ^{67}Zn and ^{119}Sn NMR fingerprints of B-type and A-type substitutions displayed by B_S and A_S compounds, respectively (Figures 2 and 3). This clearly indicates that there is no direct interaction between the [V_{Cu} + Zn_{Cu}] and [$2Zn_{Cu}$ + Zn_{Sn}] defect complexes, which coexist in the same materials but are spatially separated. Hence, the (A+B)-type compounds should rather be considered as being A-type and B-type compounds. The line widths of the main ^{119}Sn signal of $(A+B)_S$ and A_S are equal, both being smaller than those of the S_S and B_S compounds. Therefore, the presence of A-type defect complexes is associated with low-disordered [Cu,Zn] layers, regardless of the presence of B-type complexes.

A-, B-, and (A+B)-Type Substitutions Probed by Cu NMR in Slowly Cooled CZTS Samples. Let us now complete the characterization of the local structure of A- and B-type defect complexes by discussing only the ^{65}Cu NMR spectra (Figure 4). The spectrum of the S_S sample shows two resonances of equal intensity. As previously discussed by Choubrac et al.,[8] the broad line has been assigned to Cu(2a) atoms and the narrow line to Cu(2c) atoms of the ordered CZTS kesterite structure. In contrast with the ^{67}Zn and ^{119}Sn spectra discussed above, the ^{65}Cu spectra of A_S, B_S, and $(A+B)_S$ show strong similarities with the ^{65}Cu spectrum of S_S. Only slight smoothing of the right "horn" of the Cu(2a) resonance is perceptible for A_S and $(A+B)_S$ samples. These slight changes in the ^{65}Cu spectra with the composition variations could be explained by considering rearrangements of A- and B-type complexes in Cu-poor clusters with no visible NMR signal contribution.

Characterization of the Substitutions in Strongly Disordered Samples (Quenched Samples) by NMR. Figures 5−7 display the ^{65}Cu, ^{67}Zn, and ^{119}Sn NMR spectra of the CZTS samples which underwent a fast cooling to maximize the long-range Cu/Zn disorder (i.e., S_Q, A_Q, B_Q, and $(A+B)_Q$)). For all of these samples, the NMR lines experience a widening in comparison to slow-cooled analogues due to a distribution in the chemical shift for ^{119}Sn and a distribution in

dx.doi.org/10.1021/ic5012346 | Inorg. Chem. 2014, 53, 8646−8653

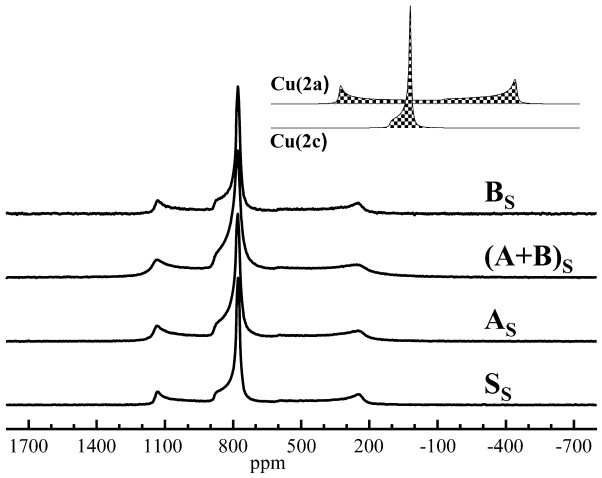

Figure 4. ^{65}Cu central transition (full shifted echo acquisition) NMR spectra acquired under static conditions at 85.2 MHz (7.05 T) of the S_S, A_S, $(A+B)_S$, and B_S samples. The inset presents the line shapes of the two ^{65}Cu sites.

both the chemical shift and the EFG for ^{67}Zn and ^{65}Cu. This is related to a more pronounced chemical disorder.[19] Practically, the existence of multiple resonances and their broadening result in a huge increase in acquisition time. This explains why only the spectrum of the (A+B)-type compound has been recorded among the nonstoichiometric quenched samples for the low-sensitivity ^{67}Zn nucleus.

As for slow-cooled samples, the ^{65}Cu spectra of the quenched nonstoichiometric samples (Figure 5) are all similar to those of

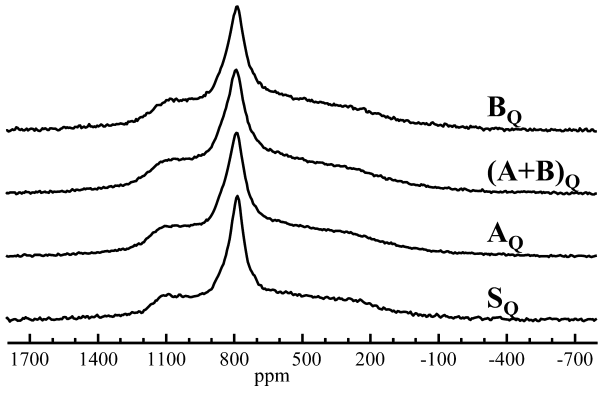

Figure 5. ^{65}Cu central transition (full shifted echo acquisition) NMR spectra acquired under static condition at 85.2 MHz (7.05 T) of the S_Q, A_Q, $(A+B)_Q$, and B_Q samples.

the stoichiometric sample, thus providing no information relative to the relationship between defect complexes and disorder. However, even if the signals are becoming more featureless, the two ^{65}Cu resonances are still clearly distinguishable. Therefore, whatever the probed composition, we can conclude that the structural type remains purely kesterite (i.e., Cu atoms at two atomic sites), with no evidence for transition toward a stannite structure type (Cu atoms at one atomic site only).

We now address the relationship between a strong Cu/Zn disorder and the defect complexes by considering ^{67}Zn and ^{119}Sn NMR spectra. In Figure 6, the evolution with disorder of the ^{67}Zn signature of the B-type complexes (the only detectable defect complex by ^{67}Zn NMR) is difficult to figure out because

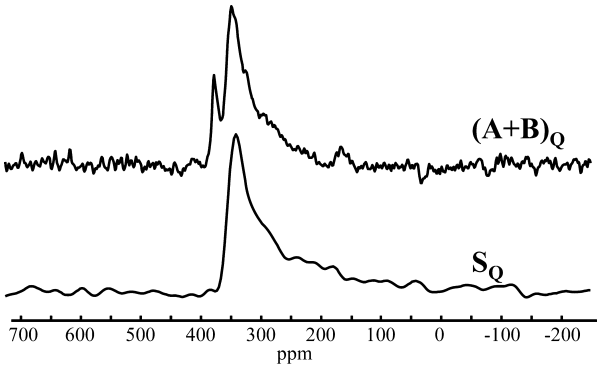

Figure 6. ^{67}Zn central transition (Hahn echo acquisition) MAS (10 kHz) NMR spectra acquired at 31.3 MHz (11.75 T) of S_Q and $(A+B)_Q$ samples.

of its overlap with the ZnS and regular CZTS signals. However, the regular CZTS signal appears wider (extending to lower frequencies) in the ^{67}Zn spectrum of S_Q than in that of $(A+B)_Q$. This broadening, mainly ascribed to an EFG distribution induced by the Cu/Zn disorder,[8] suggests a level of disorder in the $(A+B)_Q$ sample lower than that in the S_Q sample.

The impact of defect complexes on the Cu/Zn disorder is much more easily assessed through an analysis of the ^{119}Sn spectra, whose line widths reflect an isotropic chemical shift distribution. The ^{119}Sn line of B_Q (Figure 7) is only slightly

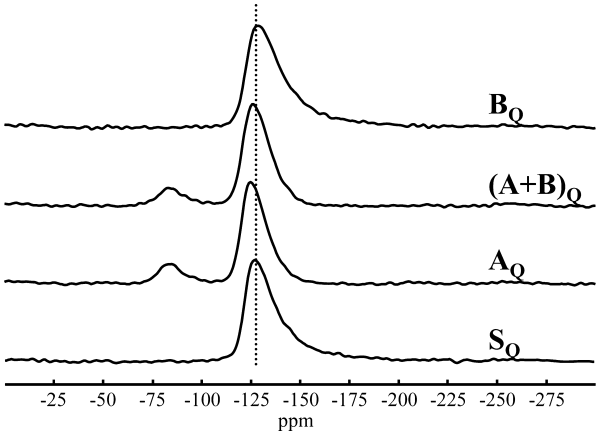

Figure 7. ^{119}Sn (full shifted echo acquisition) MAS (14 kHz) NMR spectra acquired at 111.9 MHz (7.05 T) of the S_Q, A_Q, $(A+B)_Q$, and B_Q samples.

broader than that of S_Q, but both are, of course, much broader than those of B_S or S_S. This suggests that the line width of the ^{119}Sn signal of B_Q is mainly governed by the Cu/Zn disorder. Hence, we postulate that the influence of B-type complexes on the Cu/Zn disorder is very limited or nonexistent. In contrast, the ^{119}Sn signals (at −125 ppm)[20] of the A_Q or $(A+B)_Q$ samples turn out to be narrower (and left-shifted from −127 to −125 ppm) in comparison to S_Q, fully supporting a lower level of disorder within these two samples, as suggested by ^{67}Zn spectra. This goes along with the speculation that A-type complexes (with a clear signature at ∼-80 ppm on ^{119}Sn spectra) favor a lesser level of Cu/Zn disorder in CZTS materials for quenched samples (as well as for slow-cooled samples). Of course, such defects can affect the disorder but not eliminate it. The Cu/Zn disorder is mainly driven by the

dx.doi.org/10.1021/ic5012346 | Inorg. Chem. 2014, 53, 8646−8653

synthesis procedure, as attested by the strong difference in line widths between slow-cooled and quenched samples.

The decrease in the ^{119}Sn line width from S_Q to A_Q (and $(A+B)_Q$) accounts for a reduced number of chemical surroundings experienced by these nuclei. Since the main ^{119}Sn signal at −125 ppm is not influenced by V_{Cu} at the 2a sites, the surrounding changes can only occur in the [Cu,Zn] layers. Hence, this suggests that A-type defect complexes induce specific arrangements of Cu and Zn atoms in the [Cu, Zn] layers: i.e., the distribution of Cu and Zn atoms at the 2c and 2d sites is not fully random. This is in contrast with the S_Q sample, in which a full random distribution occurs.[21] Note that in the case of the coexistence of spatially separated domains with ordered and disordered kesterite structures within a sample, the spectrum would show the superimposition of the NMR signatures of ordered and disordered domains, i.e. narrow and wide lines together, whatever the domain size involved. For the quenched samples, none of the obtained NMR spectra have shown such a superimposition.

To sum up, let us gather here the main conclusions on NMR investigations related to CZTS samples. First, a ^{119}Sn line at −81 ppm is a signature of the occurrence of A-type substitution. Analysis of this signal intensity points out the propensity of A-type defect complexes for aggregation. Second, a broad ^{67}Zn signal lying between the regular contribution of CZTS at 355 ppm and the ZnS signal at 379 ppm is assigned to B-type defect complexes. The width of this specific ^{67}Zn signal, ascribed to a chemical shift distribution due to various local enrichments in Zn atoms as second neighbors, suggests the aggregation of B-type complexes. Third, (A+B)-type substitution consists in fact of the coexistence of spatially separated A-type and B-type substitutions. Fourth, with regard to their interactions with Cu/Zn disorder, the two substitutions clearly differ in their influence. As witnessed by the width of the main ^{119}Sn resonance, $[2Zn_{Cu} + Zn_{Sn}]$ B-type defect complexes do not affect the Cu/Zn disorder in contrast to $[V_{Cu} + Zn_{Cu}]$ A-type complexes. Namely, at similar cooling rates, compounds with A-type complexes (both A-type and (A+B)-type) turn out to be less disordered than the B-type or stoichiometric S sample. However, the level of disorder is still first driven by the synthesis cooling rate.

Following this NMR investigation, Raman spectroscopy measurements were initiated on the eight previous well-characterized materials to discuss the suitability of Raman to characterize defect complexes. We also provide a new reading of the effects of Cu/Zn disorder on Raman spectra. In particular, we give evidence challenging the previous attribution of a peak near 338 cm^{-1} to Cu/Zn disorder.

Effects of Cu/Zn Disorder and A- and B-Type Substitutions on Raman Spectra. Raman spectroscopy, a very convenient method for quick analysis of thin films, is now a widespread technique commonly used to characterize CZTS materials. Though its major purpose still mainly consists of the detection of impurity phases (e.g., ZnS),[22] Raman spectroscopy may also be indicative of defects in CZTS. For instance, it is speculated that the band at 332 cm^{-1} (λ_{ex} 514 nm) is associated with Cu/Zn disorder.[23,24] On the basis of data collected at 514 nm on all our fast- and slow-cooled samples (Supporting Information, Figures S5 and S6), we can definitely ensure that this line is related neither to Cu/Zn disorder (cooling rate) nor to the substitution type, since the band at 332 cm^{-1} is very low in all cases. This peak might originate from an effect of phonon confinement, as proposed by Dimitrievska et al.[25]

Very recently, using a near-resonant excitation (785 nm), Scragg et al.[26] have shown that the intensity ratio between peaks at 287 and 303 cm^{-1} ($Q = I_{287}/I_{303}$) can be regarded as an order parameter to estimate the magnitude of random distribution of Cu and Zn at 2c and 2d crystal sites. The higher the Q factor, the lower the ability of Cu(Zn) atoms to occupy Zn(Cu) atomic sites in a random way. Here, we seized the opportunity to have at our disposal well-characterized materials to discuss further the effect of Cu/Zn disorder on Raman spectra and to investigate the potential of Raman spectroscopy for substitution-type ascertainment.

Figures 8 and 9 display the Raman spectra of slow-cooled and fast-cooled CZTS samples on excitation at 785 nm. The

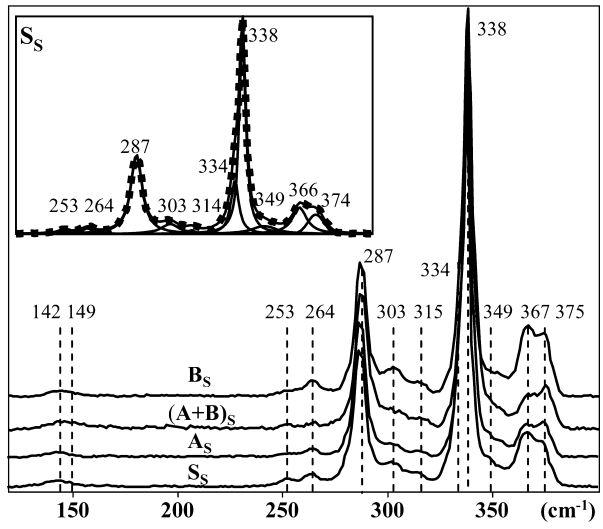

Figure 8. Normalized Raman spectra of the S_S, A_S, $(A+B)_S$, and B_S samples using 785 nm excitation wavelength. The peak positions are the mean values determined using 16 spectra (4 spectra on different spots for each sample). The inset presents the decomposition of S_S.

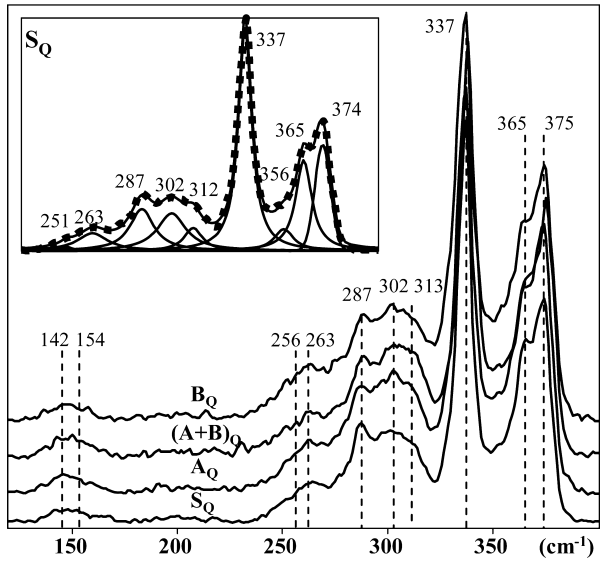

Figure 9. Normalized Raman spectra of the S_Q, A_Q, $(A+B)_Q$, and B_Q samples using 785 nm excitation wavelength. The peak positions are the mean values determined using 16 spectra (4 spectra on different spots for each sample). The inset presents the decomposition of S_Q.

dx.doi.org/10.1021/ic5012346 | Inorg. Chem. 2014, 53, 8646−8653

decompositions of the S_S and S_Q spectra with Gaussian curves are given in the insets. Namely, going from X_S to X_Q materials (X = S, A, B, (A+B)), the positioning of the Raman lines are not significantly affected (Supporting Information, Table S2) and the full width at half-maximum is increased for all of the peaks (e.g., from 4.7 to 10.5 cm^{-1} for the line at 338 cm^{-1}; see the Supporting Information, Table S3).[19] Similar conclusions can be drawn for the spectra acquired at 514 nm (Supporting Information, Figures S5 and S6 and Tables S2 and S3).

For convenience, let us now consider specifically the Raman spectra of S_S and S_Q materials (Figure 10). As one goes from an

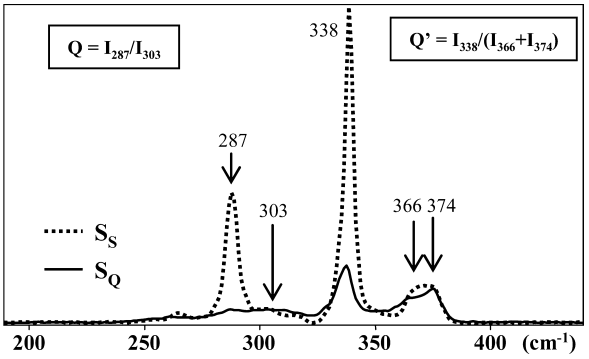

Figure 10. Non-normalized Raman spectra of the S_S and S_Q samples recorded using 785 nm excitation wavelength.

ordered stoichiometric to a disordered stoichiometric CZTS, it is worth noting that the lines at 287 and 338 cm^{-1} strongly decrease while peaks at 303, 366, and 374 cm^{-1} remain almost constant. Interestingly, the Q parameter falls from 5.1(9) to 0.9(1) from S_S to S_Q. As illustrated in Table 2, this severe

Table 2. Q and Q' Values Obtained from the Raman Spectra Recorded with 785 nm Excitation

	Q^a		Q'^a	
substitution	slow cooled	quenched	slow cooled	quenched
stoichiometric	5.1(7)	0.9(1)	2.8(2)	1.0(1)
A-type	8.2(5)	1.1(1)	3.6(2)	0.9(1)
(A+B)-type	4.8(6)	1.0(3)	3.4(1)	0.9(1)
B-type	2.4(3)	0.6(2)	2.0(1)	0.9(1)

[a]Mean values determined from four spectra recorded on different spots for each sample. Standard deviations are given in parentheses.

correlation of the Q parameter with the thermal treatment of the probed material can be extended to the A, B, and (A+B) samples. Consequently, whatever the chemical composition, the Q value can be used as a good indicator of the degree of disorder in CZTS materials. Namely, a Q value clearly higher than 1 is characteristic of an ordered material. More impressive is the ability of the Q factor to discriminate between S-type, A-type, and B-type materials for slow-cooled materials with Q values of 5.1, 8.2, and 2.4, respectively (but not between S-type and (A+B)-type). Unfortunately, such discrimination cannot be envisioned at all for fast-cooled materials, where the Q values are all around 0.9.

Still for X_S samples, we now discuss the relative intensities of the Raman lines at 366 and 374 cm^{-1}, which depend on the nature of the substitutions as displayed in Figure 8. Then, in addition to the Q parameter, we propose to introduce the additional ratio $Q' = I_{338}/(I_{366} + I_{374})$ to help in distinguishing substitution types. Calculated Q' values are given in Table 2. Q' values vary along the sequence $Q'(A_S) \approx Q'((A+B)_S) > Q'(S_S) > Q'(B_S)$. Consequently, we may clearly discriminate within a series with a low Cu/Zn disorder, between stoichiometric and nonstoichiometric compositions. Of particular interest, in contrast with the Q parameter, the Q' ratio offers here the possibility to distinguish a S-type material from an (A+B)-type material (but not a A-type from a (A+B)-type). Thus, on the basis of the examination of both Q and Q' ratios, S_S, A_S, B_S, and $(A+B)_S$ samples may be unambiguously differentiated by Raman spectroscopy only. For highly disordered samples, the Q' ratio, like the Q ratio, provides no help in discriminating S-, A-, B-, and (A+B)-type materials. We may anticipate this result may help to identify defect complexes in low-disordered CZTS thin films and to rationalize conversion performances of CZTS-based thin-film solar cells.

CONCLUDING REMARKS

Syntheses of Cu-poor, Zn-rich CZTS compounds with a good control of the chemical composition and the level of Cu/Zn disorder allowed us to improve the understanding of the structures of defect complexes and their impacts on the long-range Cu/Zn disorder. For both A- and B-type substitutions, NMR investigations demonstrated the homoclustering of the complexes. We also showed that no interaction between $[V_{Cu} + Zn_{Cu}]$ and $[2Zn_{Cu} + Zn_{Sn}]$ defect complexes exists in (A+B)-type compounds. Furthermore, we proposed that Zn environments similar to those in the ZnS (zinc blende type) structure exist locally with B-type complexes. Although the results are restricted to the samples of low level of Cu/Zn disorder, we showed that, through both Q and Q' ratios, Raman spectra recorded with 785 nm excitation can differentiate the nature of the substitution. With regard to their interactions with Cu/Zn disorder, the two substitutions clearly differ. While $[2Zn_{Cu} + Zn_{Sn}]$ complexes do not affect the disorder, $[V_{Cu} + Zn_{Cu}]$ complexes restrain the long-range Cu/Zn disorder to some extent. More importantly, this restricting effect of Cu/Zn disorder still exists when both A- and B-type defect complexes are present within a sample. Again, relying on the NMR characterization of disorder, we reinterpreted Raman spectra and showed that the intensity of the Raman peak at 332 cm^{-1} obtained with 514 nm excitation cannot account for the level of Cu/Zn disorder in the [Cu,Zn] layer. Irrespective of the sample composition, the $Q = I_{287}/I_{303}$ ratio obtained with 785 nm excitation (near-resonant conditions) is very sensitive to Cu/Zn disorder and even offers a way to estimate its level.

Drawbacks for using CZTS as the absorber layer are the possible presence of phase impurities and the band gap fluctuations originating from nonhomogeneous compositions and Cu/Zn disorder. With regard to the synthesis issues, copper sulfides and, to a lesser extent, tin sulfides are the most deleterious secondary phases for solar-cell performances. They can be avoided by using slightly off-stoichiometric B-type composition (Cu-poor, Sn-poor, Zn-rich). In addition, such a composition avoids the formation of Cu_{Zn} defects identified as deleterious for p-type doping.[5] Among the structural issues, Cu/Zn antisite defect complexes are a primary cause of band gap fluctuations. As shown in this study, the presence of A-type complexes restrains the long-range Cu/Zn disorder, even if B-type substitution also occurs within the sample. Therefore, we speculate that absorber layers for high-performance solar cells might be obtained by using (A+B)-type CZTS with a low level of Cu/Zn disorder (e.g., annealed thin films).

dx.doi.org/10.1021/ic5012346 | Inorg. Chem. 2014, 53, 8646−8653

In conclusion, we believe that, in addition to the overall information already provided in this work by NMR spectroscopy, the use of this invaluable tool can be still extended. As a first and direct application, it can be used to evaluate the A- or B-type signature detection abilities of other techniques or approaches. Another possible application is related to the Cu/Zn disorder, which could be of importance in achieving high-performance CZTS absorber layers. The recently developed near-resonant Raman approach has paved the way for the quantitative investigation of disorder and is far more convenient than NMR for thin-film materials. However, this method suffers from the need of spectral decompositions for obtaining the line intensity ratio Q used as an order parameter. As a result, the line intensity ratios can be biased and differ from the more reliable criterion offered by NMR line widths. Thus, we anticipate that NMR will be helpful in designing and calibrating the incoming Raman-based method for quantification of disorder.

■ ASSOCIATED CONTENT

Supporting Information

Text, figures, and tables giving representations of the ordered and disordered kesterite structure, details of the synthesis and chemical analyses, additional ^{119}Sn NMR spectra for A-type samples, schemes showing local changes in crystallographic environments induced by A- and B-type defect complexes, and lattice parameters, Raman spectra using 514 nm excitation, and positions and widths of the Raman lines for all of the samples. This material is available free of charge via the Internet at http://pubs.acs.org.

■ AUTHOR INFORMATION

Corresponding Author

*M.P.: e-mail, Michael.paris@cnrs-imn.fr; tel, +33 240373901; fax, +33 240373995.

Notes

The authors declare no competing financial interest.

■ ACKNOWLEDGMENTS

The technical assistance of N. Stephant and L. Nguyen for EDX analyses and of J. Y. Mevellec for Raman spectroscopy are acknowledged. The authors also acknowledge the financial support of the French ANR under Grant NovACEZ (ANR-10-HABISOL-008) and the anonymous reviewers for their nice comments.

■ REFERENCES

(1) Wang, W.; Winkler, M. T.; Gunawan, O.; Gokmen, T.; Todorov, T. K.; Zhu, Y.; Mitzi, D. B. *Adv. Energy Mater.* **2014**, *4*, 1301465.
(2) Jackson, P.; Hariskos, D.; Lotter, E.; Paetel, S.; Wuerz, R.; Menner, R.; Wischmann, W.; Powalla, M. *Prog. Photovolt. Res. Appl.* **2011**, *19*, 894−897.
(3) Polizzotti, A.; Repins, I. L.; Noufi, R.; Wei, S.-H.; Mitzi, D. B. *Energy Environ. Sci.* **2013**, *6*, 3171.
(4) Gokmen, T.; Gunawan, O.; Todorov, T. K.; Mitzi, D. B. *Appl. Phys. Lett.* **2013**, *103*, 103506.
(5) Chen, S.; Gong, X. G.; Walsh, A.; Wei, S.-H. *Appl. Phys. Lett.* **2010**, *96*, 021902.
(6) Bonazzi, P.; Bindi, L.; Bernardini, G. P.; Menchetti, S. *Can. Mineral.* **2003**, *41*, 639−647.
(7) Schorr, S.; Hoebler, H.-J.; Tovar, M. *Eur. J. Mineral.* **2007**, *19*, 65−73.
(8) Choubrac, L.; Paris, M.; Lafond, A.; Guillot-Deudon, C.; Rocquefelte, X.; Jobic, S. *Phys. Chem. Chem. Phys.* **2013**, *15*, 10722−10725.
(9) Lafond, A.; Choubrac, L.; Guillot-Deudon, C.; Deniard, P.; Jobic, S. *Z. Anorg. Allg. Chem.* **2012**, *638*, 2571−2577.
(10) Chen, S.; Walsh, A.; Gong, X. G.; Wei, S.-H. *Adv. Mater.* **2013**, *25*, 1522−1539.
(11) Bernardini, G. P.; Bonazzi, P.; Corazza, M.; Corsini, F.; Mazzetti, G.; Poggi, L.; Tanelli, G. *Eur. J. Miner.* **1990**, *2*, 219−225.
(12) Choubrac, L.; Lafond, A.; Guillot-Deudon, C.; Moëlo, Y.; Jobic, S. *Inorg. Chem.* **2012**, *51*, 3346−3348.
(13) Kentgens, A. P. M.; Verhagen, R. *Chem. Phys. Lett.* **1999**, *300*, 435−443.
(14) Massiot, D.; Fayon, F.; Capron, M.; King, I.; Le Calvé, S.; Alonso, B.; Durand, J.-O.; Bujoli, B.; Gan, Z.; Hoatson, G. *Magn. Reson. Chem.* **2002**, *40*, 70−76.
(15) Valakh, M. Y.; Dzhagan, V. M.; Babichuk, I. S.; Fontane, X.; Perez-Rodriquez, A.; Schorr, S. *JETP Lett.* **2013**, *98*, 255−258.
(16) Huang, D.; Persson, C. *Thin Solid Films* **2013**, *535*, 265−269.
(17) Bastow, T. J.; Stuart, S. N. *Phys. Status Solidi B* **1988**, *145*, 719−728.
(18) The intense contribution of ZnS to the ^{67}Zn spectrum originates from the selective nature of NMR. In NMR spectroscopy, signals from the nuclei of different isotopes (e.g., ^{67}Zn) are obtained in separate spectra. Thus, when quantitative spectra are acquired, line intensities are proportional to the total number of resonating nuclei (e.g., ^{67}Zn) of each phase and so may not be proportional to the amount of phases. The ^{67}Zn NMR line at 379 ppm represents 22% of the whole spectrum of B_S. Therefore, considering that the 379 ppm line is only associated with the ZnS phase and taking into account the molar masses of ZnS and CZTS, the corresponding amount of ZnS would be estimated around 5 wt %. However, this percentage may be overestimated due to the contribution of the specific B-type signal to the 379 ppm line (vide infra). This interpretation agrees with the 2.5 wt % of ZnS deduced from the difference between the targeted ($Cu_{1.90}Zn_{1.16}Sn_{0.945}S_4$) and experimental compositions ($Cu_{1.95}Zn_{1.06}Sn_{0.99}S_4$).
(19) In addition to the line broadening observed in both NMR and Raman spectra, the Cu/Zn disorder in the [Cu,Zn] layer can also be assessed through the c/a lattice parameter ratio derived from powder XRD (Supporting Information, Table S1). However, this approach calls for an accurate determination of the c/a ratio, which cannot be achieved in not highly crystallized samples such as thin-film materials.
(20) From slow-cooled to quenched samples, a similar right-shift (∼−4 ppm) occurs for both the −81 and the −121 ppm ^{119}Sn resonances of A-type samples, which fully supports our previous assignment of the ^{119}Sn line at −81 ppm to Sn nuclei experiencing Cu(2a) vacancies as second neighbors.
(21) Lafond, A.; Choubrac, L.; Guillot-Deudon, C.; Fertey, P.; Evain, M.; Jobic, S. *Acta Crystallogr., Sect. B: Struct. Sci., Cryst. Eng. Mater.* **2014**, *70*, 390−394.
(22) Fontané, X.; Calvo-Barrio, L.; Izquierdo-Roca, V.; Saucedo, E.; Pérez-Rodriguez, A.; Morante, J. R.; Berg, D. M.; Dale, P. J.; Siebentritt, S. *Appl. Phys. Lett.* **2011**, *98*, 181905.
(23) Valakh, M. Y.; Kolomys, O. F.; Ponomaryov, S. S.; Yukhymchuk, V. O.; Babichuk, I. S.; Izquierdo-Roca, V.; Saucedo, E.; Perez-Rodriguez, A.; Morante, J. R.; Schorr, S.; Bodnar, I. V. *Phys. Status Solidi RRL-Rapid Res. Lett.* **2013**, *7*, 258−261.
(24) Caballero, R.; Garcia-Llamas, E.; Merino, J. M.; León, M.; Babichuk, I.; Dzhagan, V.; Strelchuk, V.; Valakh, M. *Acta Mater.* **2014**, *65*, 412−417.
(25) Dimitrievska, M.; Fairbrother, A.; Pérez-Rodríguez, A.; Saucedo, E.; Izquierdo-Roca, V. *Acta Mater.* **2014**, *70*, 272−280.
(26) Scragg, J. J. S.; Choubrac, L.; Lafond, A.; Ericson, T.; Platzer-Björkman, C. *Appl. Phys. Lett.* **2014**, *104*, 041911.